 CMES, vol.22, no.1, pp.31-40, 2007

Non-Equilibrium Molecular Dynamics Simulation of Water Flow around a Carbon Nanotube

Wenzhong Tang[1] **and Suresh G. Advani**[1,2]

Abstract: In this paper, non-equilibrium molecular dynamics (MD) simulations were performed to investigate water flow around a single-walled carbon nanotube. In the simulation, the nanotube was modeled as a rigid cylinder of carbon atoms. Water molecules were described with the extended simple point charge (SPC/E) model. The nanotube-water interactions were calculated with a Lennard-Jones potential between carbon-oxygen pairs. The water-water interactions comprised a Lennard-Jones potential between the oxygen-oxygen pairs and a Coulomb potential between all charge sites on interactive water molecules. It was shown that classical continuum mechanics does not hold when the drag forces on the nanotube are considered. In slow cross flows (perpendicular to the tube axis), the cross drag on a nanotube calculated from MD simulations were larger than those from the empirical equations, and the difference increased as the flow velocity decreased. It was also found that in axial flow (in longitudinal direction), due to severe slippage on the nanotube surface, the axial drag on a nanotube from MD simulation was very small compared with the calculation from continuum mechanics.

Keyword: Molecular dynamics simulation, water flow, nanotube, drag.

1 Introduction

A circular cylinder in fluid flow has been of theoretical and experimental interest for many years [Lamb (1945), White (1946), Finn (1953), Kaplun (1957), Broersma (1960), Cox (1970), Batchelor (1970), Happel and Brenner (1973), Ui, Hussey and Roger (1984)]. One main concern of this subject was the drag force on the cylinder in a flow field. Cross drag on a circular cylinder in cross (transverse) flow and axial drag in axial (parallel) flow form the basis for studying the dynamics of flexible fibers in a suspension flow [Yamamoto and Matsuoka (1993), Ross and Klingenberg (1997), Joung, Phan-Thien and Fan (2001), Tang and Advani (2005)], which allows one to predict fiber orientation and distribution in the flowing suspension and its bulk rheological properties. In recent years, carbon nanotubes, a cylindrical fiber-like material with superior mechanical properties and large aspect ratios, have been extensively explored to reinforce various polymeric resins [Tang, Santare and Advani (2003), Gong, Li, Bai, Zhao and Liang (2004), Wu and Shaw (2004), Gojny, Wichmann, Köpke, Fiedler and Schulte (2004)]. While considerable progress has been made in the enhancement of polymer-nanotube composites, and a few viscosity measurements have been reported on nanotube suspensions [Kinloch, Roberts and Windle (2002), Pötschke, Fornes and Paul (2002), Seo and Park (2004)], little theoretical work has been done on the flow behavior and rheological properties of carbon nanotube suspensions. The major hurdle to performing the theoretical study is lack of a practical device to obtain the nano-level drag between the nanotube and the surrounding fluid molecules. To our knowledge, currently no technique is available to measure the drag on a nanotube in a liquid flow. However, molecular dynamics simulation method enables one to investigate nanotube behavior and liquid flows at the molecular level [Rapaport (1995), Todd (2001), Wei, Srivastava and Cho (2002)]. Due to the big difference in length scale, continuum theories for

[1] Department of Mechanical Engineering and Center for Composite materials, University of Delaware, Newark, DE 19716-3140, USA

[2] Corresponding author; email: advani@udel.edu

macroscale flow may not be applicable when considering similar flows at the nanoscale.

By nonequilibrium molecular dynamics simulations, Travis, Todd and Evans (1997) investigated Poiseuille flows of a fluid composed of spherical particles. They found that, in the simple fluid case, classical behavior was approached when channel width was 10.2 times the molecular diameter of the fluid particle, but when channel width reduced to 5.1 times the molecular diameter, Navier-Stokes theory began to break down. Walther, Werder, Jaffe and Koumoutsakos (2004) investigated water flow past a single walled carbon nanotube using nonequilibrium molecular dynamics simulation. It was found that slip length in the plane normal to nanotube axis was comparable to the van der Waals distance of the carbon-water potential whereas significant slip occurred along its axis. They also calculated the fluid force acting on the nanotube and, based on a few data, they reported that the cross drag forces on the nanotubes were in reasonable agreement with the Stokes-Oseen solution for macroscale cylinders.

In our previous work [Tang and Advani (2006)], we studied the cross drag on a nanotube in uniform argon flow. It was found that the calculated drag forces by molecular dynamics simulation were different from what one would expect from continuum mechanics. In the range of velocities encountered in engineering applications, the drag on a nanotube is expected to be much larger than the one calculated using continuum mechanics theory, which indirectly explains the increase in viscosity of the nanotube suspension even at small concentrations. However, one question arises from our previous study - Does our conclusion about the drag on a nanotube in liquid argon flow extend to other polyatomic fluids? In this paper, we focus on the cross and axial drag forces on a nanotube in water flow.

2 Simulation details

Water molecules flowing around a single walled zigzag (6, 0) nanotube (with a diameter of $d = 0.4752nm$) was investigated in this study. Figure 1 illustrates a unit cell of a carbon nanotube - water system used in our simulation. In the $L \times W \times H$ cubic cell, the nanotube is fixed at the center of the system, with its axis along the z direction. Around the nanotube are water molecules at 25°C, with a density of $\rho = 996kg/m^3$ and a dynamic viscosity of $\mu = 8.90 \times 10^{-4} kg/m \cdot s$ [Kundu (1990)]. The water molecule was described with the extended simple point charge (SPC/E) model as shown in Figure 2 [Berendsen, Grigera and Straatsma (1987), Kusalik and Svishchev (1994)], where the bond length ($r_{OH} = 1 \times 10^{-10} m$) and bond angle ($\angle HOH = 109.47^o$) are fixed; the oxygen carries a negative electric charge of $q_O = -0.8476e$ and each hydrogen atom carries a positive charge of $q_H = 0.4238e$; and the oxygen-oxygen well depth and van der Waals radius are $\varepsilon_{OO} = 0.6501 KJ/mol$ and $\sigma_{OO} = 3.166 \times 10^{-10} m$ respectively. The interactions between two water molecules consist of a Lennard-Jones potential between the oxygen atoms and a Coulomb potential comprising of all electrically interactive pairs. The Leonard-Jones potential between the oxygen pair is calculated as [Kotsalis, Walther and Koumoutsakos (2004)]

$$E_{LJ}(r_{OO}) = 4\varepsilon_{OO}\left[\left(\frac{\sigma_{OO}}{r_{OO}}\right)^{12} - \left(\frac{\sigma_{OO}}{r_{OO}}\right)^{6}\right], \quad r_{OO} \le r_{c\_LJ} \quad (1)$$

where r_{OO} is the distance between the two oxygen atoms and $r_{c\_LJ} = 1.0 \times 10^{-9} m$ is a cutoff distance beyond which the Lennard-Jones interaction is neglected. The Coulomb potential between two electrically interactive sites is expressed as [Kotsalis, Walther and Koumoutsakos (2004)]

$$E_{El}(r_{ij}) = \frac{q_i q_j}{4\pi\varepsilon_0 r_{ij}}, \quad r_{ij} \le r_{c\_EL} \quad (2)$$

where q_i and q_j are the electric charges of the two sites, $\varepsilon_0 = 8.854 \times 10^{-12} F/m$ is the permittivity in vacuum, r_{ij} is the distance between the two interaction sites, and r_{c_EL} is a cutoff distance beyond which the electrostatic interaction is neglected. The truncation of the Coulomb potential has been shown to have little effect on the thermodynamic and structural properties of water for cutoff distances larger than $6.0 \times 10^{-10} m$ [Andrea, Swope and Andersen (1984)].

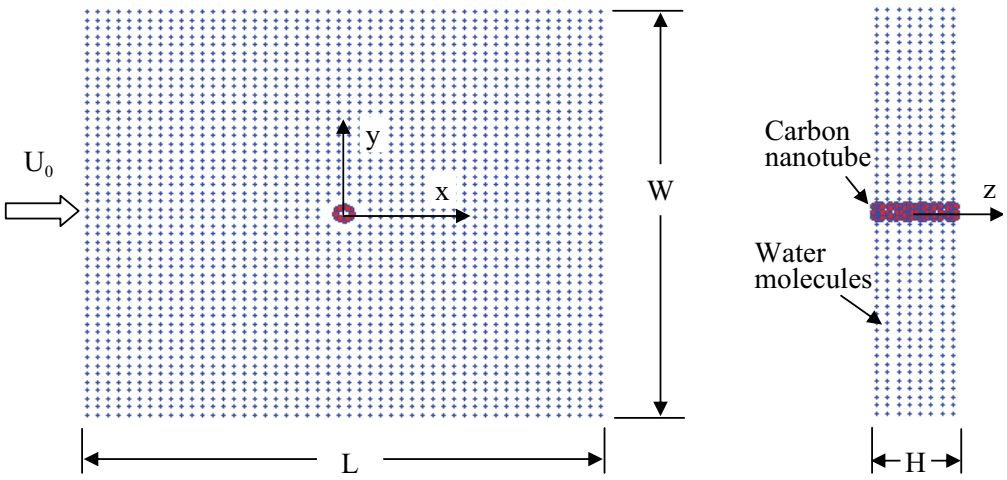

Figure 1: Unit cell of carbon nanotube – water system: (a) top view; (b) side view.

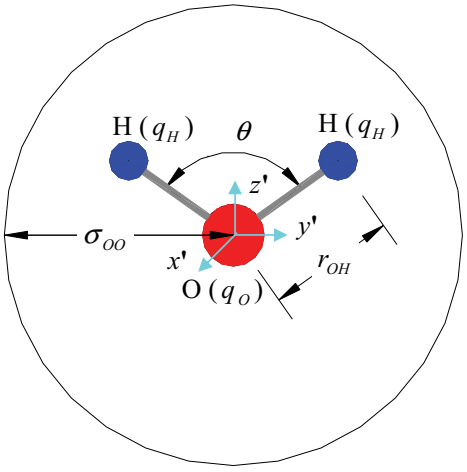

Figure 2: SPCE water model (Atoms are on the $y'z'$ plane).

In this work, we employed a cutoff distance of $r_{c\_EL} = 1.14 \times 10^{-9} m$. A larger value did not make much difference in the drag on the nanotube from our simulation. As in our previous work [Tang and Advani (2006)] and in the work by Gordillo and Marti (2003) and by Walther, Werder, Jaffe and Koumoutsakos (2004), the carbon nanotube was modeled as a rigid structure, in which the bonds between carbon atoms are fixed (bond length $r_{C-C} = 1.42 \times 10^{-10} m$) and the carbon atoms do not move relative to each other. The rigid tube model is used in our study since it has been verified that the consideration of carbon mobility has little effect on the hydrodynamic properties of water/carbon nanotube system [Werder, Walther, Jaffe, Halicioglu and Koumoutsakos (2003)]. The nanotube-water interaction is described by the Lennard-Jones potential between the carbon and oxygen sites which is expressed as

$$E_{LJ}(r_{CO}) = 4\varepsilon_{CO}\left[\left(\frac{\sigma_{CO}}{r_{CO}}\right)^{12} - \left(\frac{\sigma_{CO}}{r_{CO}}\right)^{6}\right], \quad r_{CO} \le r_{c\_LJ} \quad (3)$$

where $\varepsilon_{CO} = 0.4389 KJ/mol$ and $\sigma_{CO} = 3.19 \times 10^{-10} m$ are the carbon-oxygen well depth and carbon-oxygen van der Waals radius respectively [Bojan and Steele (1987), Werder, Walther, Jaffe, Halicioglu and Koumoutsakos (2003)], r_{CO} is the distance between the interaction sites, and $r_{c\_LJ} = 1.0 \times 10^{-9} m$ is the same cutoff distance as in Equation 1 for oxygen-oxygen pairs. With the above potentials, a code based on the one by Rapaport (1995) for two-dimensional liquid argon flow around a circular obstacle was developed to simulate the water flow around a carbon nanotube.

In this paper, two types of flow are investigated. One is cross (transverse) flow in which the flow direction is perpendicular to the axis of the nanotube, and the other is axial flow in

which the water molecules flow parallel to the tube axis. In both cases, the water molecules are initially evenly placed in the domain, and all water molecules have identical translational and rotational speeds but move in random directions resulting in a system with zero resultant velocity. A cross (transverse) flow is initialized by superimposing a desired flow velocity in the x direction on all water molecules, and maintained by first redefining random velocity of molecules within $0.025 \times L$ to the $x = -L/2$ boundary every 40 time steps, and then superimposing the desired flow velocity on these molecules. This technique of maintaining uniform flow also removes excess heat, which is equivalent to adding a heat sink at the inlet [Rapaport (1995), Tang and Advani (2006)]. An axial flow is generated in a similar way. It is initialized by superimposing a desired flow velocity in the z direction on all water molecules, and maintained by superimposing the desired velocity in the axial (z-) direction on molecules within $0.025 \times L$ to the $x = \pm L/2$ boundaries and within $0.025 \times W$ to the $y = \pm W/2$ boundaries. Periodic boundary condition was used in all three directions. In this work, neighbor list method was used in the calculation of interactions between atoms, and the equations of motion were integrated with predictor-corrector method. In our calculations, non-dimensional parameters were used by choosing σ_{OO}, ε_{OO}, and m_{H_2O} (molecular mass of water) as the units of length, energy and mass respectively, leading to a time unit of $t = 1.666 \times 10^{-12} s$. In this study, parameters will be given in the non-dimensional units (or reduced units) unless otherwise stated. Throughout this work, a time step of $6.25 \times 10^{-16} s$ was used.

3 Results and discussion

In this paper, the cross and axial drag forces on the nanotube were obtained from cross (transverse) and axial (parallel) flow respectively. Drag forces from MD simulations were compared with classical results from empirical equations for flow around a circular cylinder.

3.1 Cross (transverse) flow

3.1.1 Time-averaged cross drag

To obtain the cross drag on the nanotube in the cross flow, simulations were performed until the system reached steady state and maintained the state for a series of additional time steps. The number of time steps needed for a run varied from 800,000 to 1,600,000. When a lower flow speed U_0 was applied, more time steps were needed for the system to reach steady state. Figure 3 shows typical results of total, kinetic and potential energy of the system as a function of time. In this case, the nanotube was placed in a domain of $L \times W \times H = 13.26 \times 13.26 \times 0.85 nm^3$ and a flow speed $U_0 = 95 m/s$ (or 0.5 in reduced units) was applied. We observed that both kinetic and potential energy decreased during the inception stage. The kinetic energy decreased because initially a flow velocity of U_0 was superimposed on all water molecules. Due to resistance from the nanotube, the flow slowed down with time until the input of imposed flow balanced the resistance due to the presence of the nanotube; thus the system reached steady state after $t = 150$. At each time step, the drag force on the nanotube (instantaneous drag) was obtained by summing up forces on all carbon atoms. Figure 4a presents the instantaneous drag as a function of time. To characterize the drag on the nanotube, time-averaged values were obtained by averaging the instantaneous drag over time. The time-averaged drag $F_d^{avg}(t)$ was calculated as

$$F_d^{avg}(t) = \frac{1}{N_{t_0-t}} \sum_{t_0}^{t} F_d(t), \tag{4}$$

where t_0 was chosen as a fixed starting time when the system was at steady state, t is any time after t_0, and N_{t_0-t} is the number of sampling points from t_0 to t. Figure 4b shows the time-averaged drag when the starting time t_0 = 200. It is seen that the time-averaged drag converges with time, resulting in an average value of 79.73 and a standard deviation of 0.26 for t = 400 $\sim$ 450. In this work, the time-averaged value from t_0 (vary from 200 to 400) to the end of each simulation t_{end}(vary from 450 to 600) will be used to characterize the drag force on the nanotube.

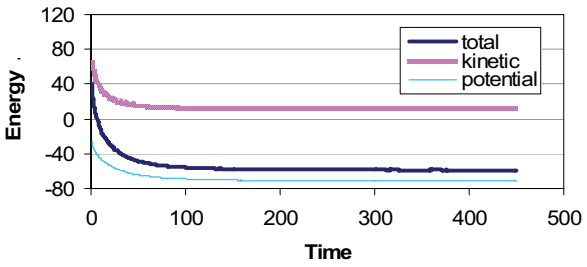

Figure 3: Energy development in a water-nanotube flowing system (in reduced units)

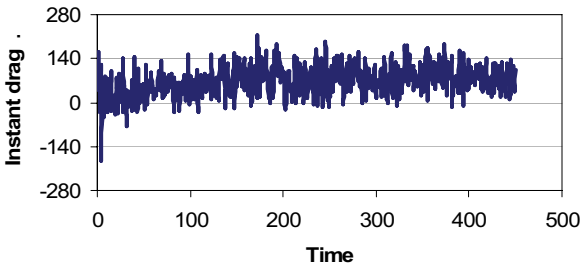

(a)

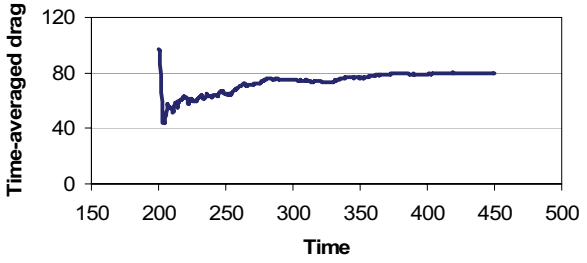

(b)

Figure 4: Typical simulated drag on a nanotube (in reduced units): (a) instantaneous drag; (b) time-averaged drag.

3.1.2 Effect of domain size on cross drag

Due to the time consuming nature of molecular dynamic simulations, a small system is desirable but a system too small may provide inaccurate information. Our idea was to use a small cell thickness H to speed up our calculation. The simulation time is approximately proportional to the size of the system. When the cell thickness H is reduced, the number of molecules in the system reduces, requiring less calculation time. Table 1 lists the unit drag (drag force per unit length) on the nanotube for 4 different values of cell thickness H while the other dimensions were fixed ($L \times W = 4.59 \times 4.59 nm^2$) when a flow speed of $U_0 = 0.5$ ($95 m/s$) was applied. It should be noted that the unit cell is repeated in all the three directions (x, y and z) due to the periodic boundary condition, so a molecule in the unit cell has its image in each of the repeating cells [Rapaport (1995)]. When the cell thickness H is small ($\leq r_{c\_EL}$), the distance between a molecule and its image in a repeating cell may fall within the interaction range, hence this interaction should also be included. It is seen when the cell thickness is larger than the cutoff distance ($H/r_{c\_EL} = 1.12$ and 2.25), the difference in the simulated unit drag force is very small (0.28%). The difference increases as the cell thickness decreases. Using the thickest cell as a reference ($H/r_{c\_EL} = 2.25$), the errors in the simulated drag are 3.4% and 68.1% for the thinner cells with $H/r_{c\_EL} = 0.75$ and 0.38 respectively. Considering both calculation time and accuracy, the cell thickness $H = 0.85 nm$ ($H/r_{c\_EL} = 0.75$) was used in our parametric study.

To examine the effect of domain size $L \times W$ on cross drag, two flow speeds $U_0 = 0.5$ ($95 m/s$) and 1.0 ($190 m/s$) and five domain sizes (L/d=11.2, 16.7, 22.3, 27.9 and 33.5, with$L = W$) were considered. Figure 5 shows that the unit drag on the nanotube decreases and converges with growing domain size for both flow speeds. The differences in drag force between the last two points on the curves are 0.99% and 3.4% for $U_0 = 0.5$ and 1.0 respectively. We settled on a domain size of $L/d = 27.9$ ($L \times W \times H = 13.26 \times 13.26 \times 0.85 nm^3$) to investigate how the cross drag changes with the flow speed.

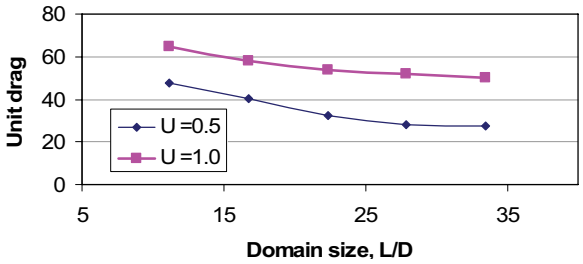

Figure 5: Convergence of drag force (in reduced units) with growing domain size.

Table 1: Cross drag on the nanotube for different cell thicknesses H ($L \times W = 4.59 \times 4.59 nm^2$, flow speed $U_0 = 95\ m/s$).

Cell thickness H, nm	0.43	0.85	1.28	2.56
(H/r_{c_EL})	(0.38)	(0.75)	(1.12)	(2.25)
Unit drag	118.0	72.4	70.4	70.2
(error, %)	(68.1)	(3.4)	(0.28)	(0.0)

3.1.3 Cross drag as a function of flow speed

To examine the effect of flow speed on the cross drag, simulations were performed on a domain size of $L \times W \times H = 13.26 \times 13.26 \times 0.85 nm^3$. The system had 4976 water molecules and 48 carbon atoms. The initial random speed of water molecules was $U_i = 3.38$ $(642.2 m/s)$ at a temperature of $T = 25^{o}$C. The flow speed U_0 was varied from 0.25∼2.5 (47.5 to $475 m/s$), corresponding to a Reynolds number of $Re = 0.025 \sim 0.25$ (based on the diameter of the nanotube). Table II lists the simulated drag per unit length F_d and drag coefficient C_d at different flow speeds. The drag coefficient was calculated as [Kundu (1990)]

$$C_d = \frac{F_d}{\frac{1}{2}\rho U_0^2 d} \quad , \tag{5}$$

where ρ is the density of water, and d is the diameter of the nanotube. It should be noted that since periodic boundary condition is used in our MD simulation, the actual problem is flow around an array of carbon nanotubes. However, as illustrated in Figure 5, the simulated drag converges as domain size increases, implying that a converged drag from a large unit cell can also be approximated as unbounded flow around a single nanotube. To compare our simulated drag with continuum theory, the drag and drag coefficient were also calculated using two empirical equations: Stokes-Oseen drag and Huner drag. The Stokes-Oseen drag is for flow past an array of two-dimensional circular cylinders and the drag coefficient is calculated as [Probstein (1989), Walther, Werder, Jaffe and Koumoutsakos (2004)]

$$C_d^{Oseen} = C_d^{cc} \frac{3 + 2\phi^{5/3}}{3 - \frac{9}{2}\phi^{1/3} + \frac{9}{2}\phi^{5/3} - 3\phi^2}, \tag{6}$$

where $\phi = \pi d^2/4LW$ is the volume fraction of the nanotube in the unit cell, and C_d^{cc} is the drag coefficient on a single circular cylinder given by

$$C_d^{cc} = \frac{8\pi}{Re \ln(7.4/Re)}. \tag{7}$$

The Huner drag, which is based on experiments using macroscale cylinders, is expressed as [Huner and Hussey (1977)]

$$F_d = F_{dLamb} \left\{ 1 - 0.87\varepsilon^2 + 0.514 \left[1 - \exp(-Re) \right] \varepsilon^3 \right\}, \tag{8}$$

where F_{dLamb} is the Lamb drag given by

$$F_{dLamb} = 4\pi\mu U_0 \varepsilon, \tag{9}$$

where μ is fluid viscosity, and ε is calculated as

$$\varepsilon = \left[0.5 - \gamma - \ln(Re/8) \right]^{-1}, \tag{10}$$

in which γ =0.577216 is Euler's constant and Re is Reynolds number. Table 2 shows that, similar to what happens at the macroscale, the cross drag force on the nanotube from MD simulation increases with the flow speed U_0 while the drag coefficient increases as the flow speed decreases. Figures 6 compares the drag coefficients calculated from MD simulation and from the empirical equations. When a flow speed of U_0=0.25 (47.5 m/s) is applied, the simulated drag (or drag coefficient) is 75% larger than the Huner and 54% larger than the Stokes-Oseen drag (or drag coefficient). As shown in Figure 6, the differences are expected to increase as the flow speed decreases. However, when the flow speed increases, the drag coefficient from MD reduces faster than that from the empirical equations. This difference in cross drag force (or drag coefficient) between MD simulation and empirical equations is similar to what we observed in our previous simulation on nanotube in liquid argon flow [Tang and Advani

Table 2: Cross drag forces (reduced units) and drag coefficients from MD simulation and empirical equations.

Flow speed U_0	Re	Drag force (Drag coefficient)		
		$F_d^{md}(C_d^{md})$	$F_d^{Huner}(C_d^{Huner})$	$F_d^{Oseen}(C_d^{Oseen})$
0.25	0.025	14.80 (297.9)	8.474 (170.6)	9.634 (194.0)
0.5	0.050	30.59 (154.0)	19.12 (96.38)	21.95 (110.5)
1.0	0.076	52.57 (66.12)	43.93 (55.28)	50.97 (64.14)
1.5	0.101	60.70 (33.95)	72.02 (40.28)	84.43 (47.22)
2.0	0.202	71.65 (22.54)	102.7 (32.32)	121.6 (38.24)
2.5	0.252	78.30 (15.76)	135.7 (27.32)	162.0 (32.62)

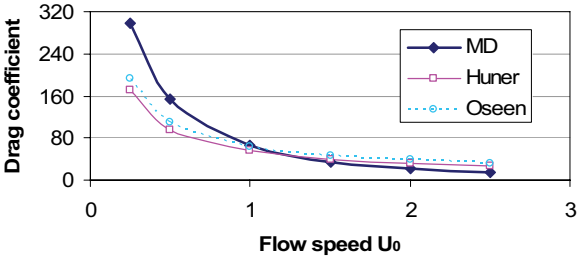

Figure 6: Comparison of drag coefficients from molecular dynamics simulation and empirical equations derived from continuum mechanics.

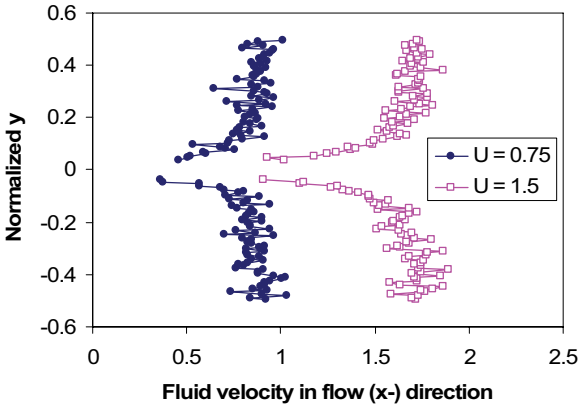

Figure 7: Velocity profile on the yz-plane through tube axis illustrating slip velocity on the nanotube surface.

(2006)]. It can be concluded that empirical equations for cross drag force on macroscale cylinders does not translate to the scale of the carbon nanotubes. Figure 7 plots the fluid velocity in the flow (x-) direction as a function of y on the yz plane through the nanotube axis (Figure 2) when flow speeds are 0.75 and 1.5. The details of how the velocity profiles are obtained can be found elsewhere [Tang and Advani (2006)]. It is seen that there is nonzero velocity on the nanotube surface, implying that slippage occurs on the tube wall. For a higher flow speed, this nonzero wall velocity (slip velocity) is larger. This explains why the drag coefficient from MD simulations reduces faster than that from the empirical equations as the flow speed increases.

3.2 Axial (parallel) flow

The axial drag was obtained on a unit cell of $L \times W \times H = 7.96 \times 7.96 \times 0.85 nm^3$, which contained 48 carbon atoms and 1776 water molecules. The simulation was performed in a similar way to the cross flow, except that the flow was in the longitudinal (z) direction of the nanotube and maintained by superimposing a desired flow velocity U_0 on molecules within $0.025 \times L$ to the $x = \pm L/2$ boundaries and within $0.025 \times W$ to the $y = \pm W/2$ boundaries (shaded regions in Figure 8a). The simulated axial drag is not sensitive to the increase in the domain size $L \times W$ or the domain thickness H. For qualitative comparison, the unit drag on a circular cylinder of infinite length moving parallel to its axis in a coaxial cylindrical boundary (Figure 8b) was also calculated using Happel and Brenner's equation [Happel and H. Brenner (1973), Ui, Hussey and Roger (1984)]

$$F_d^{Happel} = 2\pi\mu U \frac{\sigma^2 - 3 + [4(\ln\sigma)/(\sigma^2-1)]}{[(\sigma^2+1)/(\ln\sigma)] - 1}, \tag{11}$$

where μ is the dynamic viscosity of the fluid, U is the moving speed of the cylinder, and $\sigma = L/D$

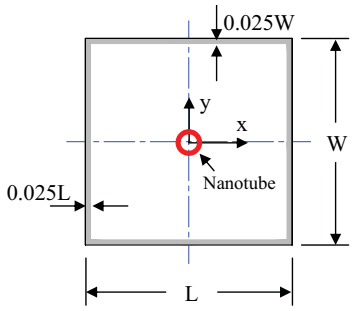

(a)

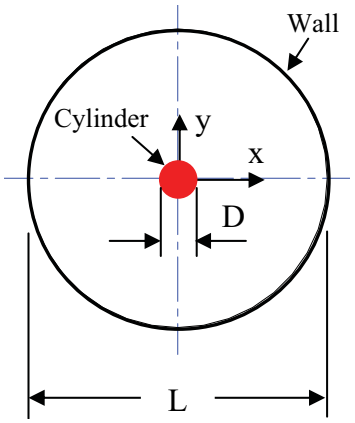

(b)

Figure 8: Domain for axial flow: (a) MD simulation; (b) Happel equation.

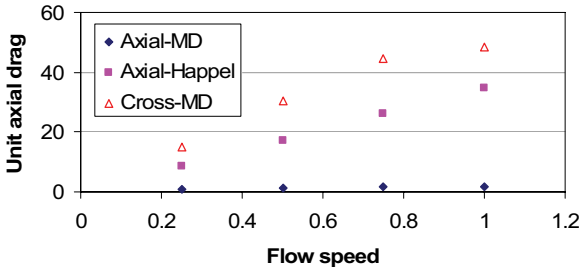

Figure 9: Drag force per unit length on the nanotube.

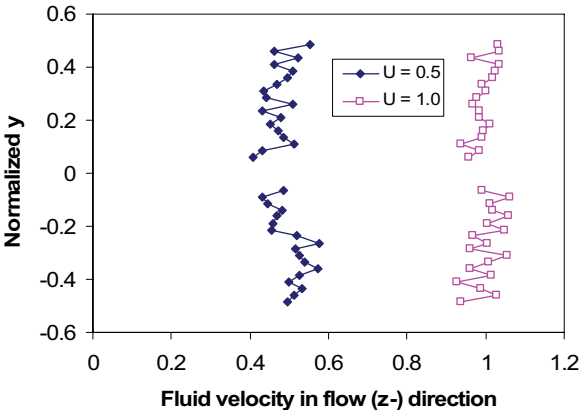

Figure 10: Velocity profile (axial flow) on the *yz*-plane through tube axis illustrating slipage on the surface of the nanotube.

is the ratio of the diameter of the flow field to the diameter of the moving cylinder. Figure 9 compares the axial drag on the nanotube from MD simulation and the above equation, in which the simulated cross drag is also plotted. It is seen the simulated axial drag forces are very small compared with the values calculated from the Happel and Brenner's equation. Figure 10 plots the velocity (flow direction) profile on the *yz* plane through the nanotube axis for flow speeds of $U_0 = 0.5$ (95 m/s) and 1.0 (190 m/s). It is shown that the magnitude of the fluid velocity on the tube wall is of the order of the applied flow speed, implying that significant slippage occurs on the surface of the nanotube in the axial flow. This explains the small axial drag forces on the nanotubes from MD simulation. Figure 9 also shows that the axial drag is negligible compared with the cross drag on the nanotube at the same flow speed.

4 Conclusions

In this work, nonequilibrium MD simulations were performed to investigate water flow around a carbon nanotube. It was found that the drag forces on the nanotube were different from what one would expect from continuum mechanics. The results show that when the flow speed was low, the cross drag coefficient from MD simulation was larger than the ones calculated from empirical equations based on continuum mechanics. The difference increased as the flow speed decreased. As the flow velocity was increased, the simulated drag from MD reduced faster and fell below the empirical results. This was attributed to slippage of the water molecules on the nanotube at large flow speeds. Above conclusions about cross drag on a nanotube in water flow disagree with what was reported by Walther, Werder, Jaffe and Koumoutsakos (2004) while agree with the con-

clusions in our previous work on nanotube in liquid argon flow. It was also shown that, due to significant slippage on the nanotube surface in axial flow, the axial drag on a nanotube from MD simulation was very small compared with the calculation from continuum mechanics. Results also show that the axial drag on the nanotube is negligible in comparison with the cross drag at the same flow speed.

Acknowledgement: This work was financially supported by the National Science Foundation on 'Processing of Nanotubes Using Liquid Composite Molding Techniques' under grant no. DMI-0115127.

References

Andrea, T. A.; Swope, W. C.; Andersen, H. C. (1984): The role of long ranged forces in determining the structure and properties of liquid water. *J. Chem. Phys*, vol. 79, pp. 4576-4584.

Batchelor, G. K. (1970A): Slender-body theory for particles of arbitrary cross-section in Stokes flow. *J. Fluid Mech*, vol. 44, pp. 419-440.

Berendsen, H. J. C.; Grigera, J. R.; Straatsma, T. P. (1987): The missing term in effective pair potentials. *J. Phys. Chem*, vol. 91 , pp. 6269-6271.

Bojan, M. J.; Steele, W. A. (1987): Interactions of diatomic molecules with graphite. *Langmuir*, vol. 3, pp. 1123-1127.

Broersma, S. (1960): Viscous force constant for a closed cylinder. *J. Chem. Phys*, vol. 32, pp. 1632-1635.

Cox, R. B. (1970): The motion of long slender bodies in a viscous fluid Part 1: General theory. *J. Fluid Mech*, vol. 44, pp. 791-810.

Finn, R. K. (1953): Determination of the drag on a cylinder at low Reynolds numbers. *J. Appl. Phys*, vol. 24, pp. 771-773.

Gojny, F. H.; Wichmann, M. H. G.; Köpke, U.; Fiedler, B.; Schulte, K. (2004): Carbon nanotube-reinforced epoxy-composites: enhanced stiffness and fracture toughness at low nanotube content. *Composites Sci. Tech*, vol. 64, pp. 2363-2371.

Gong, Q. M.; Li, Z.; Bai, X. D.; Li, D.; Zhao, Y.; Liang, J. (2004): Thermal properties of aligned carbon nanotube/carbon nanocomposites. Mater. sci. eng. A – Structural mater. properties microstructure & processing, vol. 384, pp. 209-214.

Gordillo, M. C.; Marti, J. (2003): Water on the outside of carbon nanotube bundles. *Phys. Rev. B*, vol. 67, article no. 205425.

Happel, J.; Brenner H. (1973): Low Reynolds number hydrodynamics. Noordhoff International Publishing, Leyden, Netherlands.

Huner, B.; Hussey, R. G. (1977): Cylinder drag at low Reynolds number. *Phys. Fluids*, vol. 20, pp. 1211-1218.

Joung, C. G.; Phan-Thien, N.; Fan, X. J. (2001): Direct simulation of flexible fibers. *J. Non-Newtonian Fluid Mech*, vol. 99, pp. 1-36.

Kaplun, S. (1957): Low Reynolds number flow past a circular cylinder. *J. Math. Mech*, vol. 6, pp. 595-603.

Kinloch, I. A.; Roberts, S. A.; Windle, A. H. (2002): A rheological study of concentrated aqueous nanotube dispersions. *Polymer*, vol. 43, pp. 7483-7491.

Kotsalis, E. M.; Walther, J. H.; Koumoutsakos, P. (2004): Multiphase water flow inside carbon nanotubes. *Inter. J. Multiphase Flow*, vol. 30, pp. 995-1010.

Kundu, P. K. (1990): *Fluid Mechanics*. Academic Press, California, USA.

Kusalik, P. G.; Svishchev, I. M. (1994): The spatial structure in liquid water. *Science*, vol. 265, pp. 1219-1221.

Lamb, S. H. (1993): *Hydrodynamics*. Dover Publications, New York, USA.

Pötschke, P.; Fornes, T. D.; Paul, D. R. (2002): Rheological behavior of multiwalled carbon nanotube/polycarbonate composites. *Polymer*, vol. 43, pp. 3247-3255.

Probstein, R. F. (1989): *Physicochemical Hydrodynamics*. Butter-worths, London.

Rapaport, D. C. (1995): *The Art of Molecuar Dy-*

namics Simulation. Cambridge University Press, New York, USA.

Ross, R. F.; Klingenberg, D. J. (1997): Dynamic simulation of flexible fibers composed of linked rigid bodies. *J. Chem. Phys*, vol. 106, pp. 2949-2960.

Seo, M. K.; Park, S. J. (2004): Electrical resistivity and rheological behaviors of carbon nanotubes-filled polypropylene composites. *Chem. Phys. Lett*, vol. 395, pp. 44-48.

Tang, W.; Advani, S. G. (2005): Dynamic simulation of long flexible fibers in shear flow. *CMES: Computer Modeling in Engineering & Sciences*, vol. 8, pp. 165-176.

Tang, W.; Advani, S. G. (2006): Drag on a nanotube in uniform liquid argon flow. *J. Chem. Phys*, vol. 125, article no. 174706.

Tang, W.; Santare, M. H.; Advani, S. G. (2003): Melt processing and mechanical property characterization of multi-walled carbon nanotube/high density polyethylene (MWNT/HDPE) composite films. *Carbon*, vol. 41, pp. 2779-2785.

Todd, B. D. (2001): Computer simulation of simple and complex atomistic fluids by nonequilibrium molecular dynamics techniques. *Computer Phys. Communications*, vol. 142, pp. 14-21.

Travis, K. P.; Todd, B. D.; Evans, D. J. (1997): Poiseuille flow of molecular fluids. *Physica A: Statistical & Theoretical Phys*, vol. 240, pp. 315-327.

Ui, T. J.; Hussey, R. G.; Roger, R. P. (1984): Stokes drag a cylinder in axial motion. *Phys. Fluids*, vol. 27, pp. 787-795.

Walther, J. H.; Werder, T.; Jaffe, R. L.; Koumoutsakos, P. (2004): Hydrodynamic properties of carbon nanotubes. *Phys. Rev. E*, vol. 69, article no. 062201.

Wei, C. Y.; Srivastava, D.; Cho, K. (2002): Molecular dynamics study of temperature dependent plastic collapse of carbon nanotubes under axial compression. *CMES - Computer Modeling in Engineering & Sciences*, vol. 3, pp. 255-261.

Werder, T.; Walther, J. H.; Jaffe, R. L.; Halicioglu, T.; Koumoutsakos, P. (2003): On the water-carbon interaction for use in molecular dynamics simulations of graphite and carbon nanotubes. *J. Phys. Chem. B*, vol. 107, pp. 1345-1352.

White, C. M. (1946): The drag of cylinders in fluids at slow speeds. *Proceedings Royal Soc. London, Series A, Math. Phys. Sci*, vol. 186, pp. 472-479.

Wu, M.; Shaw, L. L. (2004): On the improved properties of injection-molded, carbon nanotube-filled PET/PVDF blends. *J. Power Sources*, vol. 136, pp. 37-44.

Yamamoto, S.; Matsuoka, T. (1993): A method for dynamic simulation of rigid and flexible fibers in a flow field. *J. Chem. Phys*, vol. 98, pp. 644-650.